



Investigation on heat transfer and ablation mechanism of CFRP by different laser scanning directions

Peng Wang ^a, Zhen Zhang ^{b,c,e,*}, Bo Hao ^a, Shichuan Wei ^b, Yu Huang ^d, Guojun Zhang ^d

^a School of Mechanical Engineering and Automation, Northeastern University, Shenyang, 110819, Liaoning, China

^b School of Aerospace Engineering, Huazhong University of Science and Technology, Wuhan, 430074, Hubei, China

^c HUST Industrial Technology Research Institute, Guangdong Provincial Key Laboratory of Digital Manufacturing Equipment, Dongguan, 523808, Guangdong, China

^d State Key Laboratory of Intelligent Manufacturing Equipment and Technology, School of Mechanical Science and Engineering, Huazhong University of Science and Technology, Wuhan, 430074, Hubei, China

^e Key Laboratory of Icing and Anti/De-icing, China Aerodynamics Research and Development Center, Mianyang, 621000, Sichuan, China



ARTICLE INFO

Keywords:

Ablation
CFRP
Heat transfer
Nanosecond laser
Thermal damage

ABSTRACT

Carbon fiber reinforced plastic (CFRP) is widely applied to aviation, medical, and motorbike industry fields, thanks to its excellent performances of mechanical properties and corrosion resistance. Nanosecond pulsed laser is an efficient method for machining microchannels and holes in CFRP plates. The anisotropic heat transfer of CFRP leads to a complex mechanism of laser machining under different scanning directions (0°, 30°, 45°, 60°, 90°). A numerical model considering heterogeneity and anisotropy of nanosecond laser processing CFRP was established by COMSOL Multiphysics. By comparison of simulation and experiments under different scanning directions, the deviation of microchannel width between simulation and experimental ranges from 5.01% to 16.99%. The ablation mechanism of laser processing CFRP under different scanning directions was investigated. It demonstrates that the width of the heat affected zone (HAZ) and ablation increases with the scanning angle increasing, while decreasing with the scanning speed increasing. In addition, when compared to the scanning direction of 90°, the processing efficiency increases by 55.36%, while the width of the HAZ decreases by 55.01% when compared to the scanning direction of 0°. An optimal laser scanning speed of 630 mm/s is used to obtain the open hole with minimal HAZ and thermal damage.

1. Introduction

Carbon fiber reinforced plastics (CFRP) is an excellent composite widely applied to aerospace, automobile, sports equipment, and medical fields owing to its perfect fatigue resistance, excellent chemical resistance, and superior stiffness [1–3]. In the assembly process, many holes or grooves are essential for CFRP parts to meet the assembly requirements [4]. Since CFRP composed of carbon fiber and epoxy resin has obvious heterogeneous characteristics, it is very difficult to achieve high-quality CFRP holes with high efficiency [5].

In order to realize the processing of high-quality CFRP holes to meet the needs of assembly, researchers have conducted much research. Traditional machining methods are the most common and least costly methods for processing CFRP [6]. The CFRP machined surface has serious delamination and carbon fiber burrs during the machining process. Fibers are pulled out due to the large cutting force, which limits the application for drilling CFRP [4,7]. Cao et al. [8] proposed and implemented a bidirectional drilling process for CFRPs holes, which reduced delamination damage of the hole exit by 11.3%–27.9%.

compared to conventional drilling methods. Some researchers have proposed non-traditional processing methods, including electrical discharge machining (EDM), abrasive water jet machining (AWJM), laser machining, and laser-induced plasma micromachining (LIPMM), etc. EDM is a non-contact processing method that removes the CFRP material through the high temperature generated by the discharge between the two electrodes and obtains a perfect processed surface [9,10]. However, frequent electrode replacement results in reducing efficiency and increasing time-consuming during the EDM machining of CFRP. The AWJM is applied to machine CFRP with a smooth surface, though serious delamination and carbon fiber pull-out reduce the mechanical properties of CFRP [11].

Laser machining is a non-contact processing method [12,13], which has the advantages of high processing precision, high processing efficiency, and no tool wear, so it is widely used in machining parts with complex shapes and difficult-to-machine materials [14]. Compared with other nontraditional machining methods, including abrasive water jet machining (AWJM), ultrasonic machining (USM), and electrical

* Corresponding author at: School of Aerospace Engineering, Huazhong University of Science and Technology, Wuhan, 430074, Hubei, China.

E-mail addresses: jameszhang19880@gmail.com, zhen@hust.edu.cn (Z. Zhang).

discharge machining (EDM), laser processing is a high-quality method for processing CFRP, which has the characteristics of small HAZ, high processing precision, and high processing efficiency [15,16]. Therefore, laser processing is an ideal method for machining CFRP. The mechanism of laser processing is based on the principle of thermal ablation, which leads to HAZ and thermal damage [17,18]. Researchers have conducted related experimental studies to reduce the HAZ and thermal damage of laser-processed CFRP. Tao et al. [19] investigated the quality of laser processing CFRP in air and vacuum. The results showed that in a vacuum environment, the recoil pressure improves the mechanical removal efficiency, increases the instantaneous processing temperature, and reduces the average temperature in the processing zone. Therefore, laser processing of CFRP in a vacuum environment can significantly improve processing efficiency and reduce HAZ. The formation of HAZ can be significantly reduced by using a high-power short-pulse laser to process CFRP [20]. Leone et al. [21] applied a pulse laser with a power of 4.5 kW to machine CFRP with a thickness of 1.3 mm. By optimizing the pulse power and overlap coefficient, narrow kerfs (less than 200 μm) and small HAZ (about 0.5 mm) were obtained. For the CFRP with the characteristic of anisotropic heat transfer, researchers have revealed the mechanism of laser materials removal based on numerical simulation. The material removal rate (MRR) of carbon fiber and epoxy resin is significantly different, which results in the lower surface quality of laser-processed CFRP. Ohkubo et al. [22] analyzed the influence of the difference between the ablation rate of carbon fiber and epoxy resin on the machining quality through simulation. The corrosion rate of carbon fiber was faster than that of epoxy resin at the first stage because of the faster thermal conductivity of carbon fiber. Moreover, the resin was ablated faster due to the low evaporation temperature of epoxy resin. The quality of laser-processed CFRP is also related to processing parameters. Yang et al. [23] studied the effects of laser energy density, spot overlap rate, and adjacent scanning spacing on material removal efficiency and substrate temperature during laser paint removal based on the finite element (FE) method. The results revealed that the superposition of adjacent pulse energy can significantly improve processing efficiency. Contuzzi et al. [24] investigated the effect of laser ablation process parameters on the ablation depth and surface quality of CFRP plate by simulation analysis. The experiment results showed that excellent surface conditions were achieved with the x-parallel laser scanning strategy. The surface quality and processing efficiency of laser processing CFRP were significantly improved by optimizing the laser processing parameters, revealing the material removal mechanism and thermal damage formation mechanism.

As mentioned above, researchers conducted many experiments on laser processing CFRP to reveal the mechanism of material ablation and improve the quality of laser processing CFRP. Because the CFRP plate has anisotropy characteristics, different angles between the scanning path and the carbon fiber direction lead to different heat transfers during the laser processing CFRP, eventually leading to different ablation morphology, thermal damage, and HAZ. Although some numerical simulation about the ablation mechanism and HAZ was performed [25], there is no simulation analysis about the influence of laser scanning direction and scanning speed on the ablation mechanism from the micro level. In order to reveal the mechanism of laser CFRP from a micro level, a model of laser-processed anisotropic CFRP was established based on COMSOL Multiphysics in this paper, and the behavior of laser ablation CFRP under different scanning directions was analyzed. Combining with experiments, the relationships between different laser scanning directions and ablation depth, ablation width, and HAZ were revealed, and the process parameters were optimized with the goal of machining quality.

In the present study, a mathematical model of nanosecond pulsed laser processing CFRP considering heterogeneity and anisotropy was established, which helps to reveal the heat transfer mechanism of carbon fibers under different laser scanning directions. Moreover, the ablation mechanism of laser processing CFRP under different scanning directions and speeds on surface quality, HAZ, and thermal damage was investigated by numerical simulation and experiment analysis.

Table 1
Laser system characteristics and processing parameters.

Characteristics	Symbol	Values	Units
Wavelength	λ	355	(nm)
Repetition frequency	F	60	(kHz)
Pulse duration	τ	16.8	(ns)
Focused spot diameter	d_0	35	(μm)
Average power	P	25	(W)
Scanning speed	v	430,530,630,730,830	(mm/s)
Scanning direction	θ	0,30,45,60,90	($^{\circ}$)

Table 2
Properties of the CFRP material [20,23,26].

Property	Carbon fiber	Epoxy resin	Units
Volume fraction	60%	40%	–
Diameter	6	–	μm
Density	1850	1250	kg/m^3
Specific heat capacity	710	1884	$\text{J}/\text{kg} \text{ }^{\circ}\text{C}$
Thermal conductivity (k_{xx} , k_{yy} , k_{zz})	50;5;5	0.2	$\text{W}/(\text{m k})$
Heat of latent	43 000	1000	kJ/kg
Vaporization temperature	3900	698	K

2. Experimental procedure

2.1. Experimental materials and laser system

A nanosecond laser system is used in this experiment of laser processing CFRP by Wuhan Huaray Laser Co. Ltd, as shown in Fig. 1. And the specific parameters of the laser system are presented in Table 1. The experiments were carried out on a CFRP 1.0 mm thickness, which was composed of carbon fiber (the volume ratio: 60%) and epoxy resin matrix (the volume ratio: 40%). The carbon fibers of CFRP have an orientation sequence of 0°/90° and the diameter of the carbon fiber in the material is 6 μm , as shown in Fig. 2(a). And samples of 30 mm×30 mm were obtained by diamond saw cutting. The thermal conductivity of fiber axial direction, fiber radial direction, and epoxy resin is 50 $\text{W}/(\text{m k})$, 5 $\text{W}/(\text{m k})$, and 0.2 $\text{W}/(\text{m k})$, respectively, which leads to anisotropic heat transfer [23]. Other mechanical and physical properties of CFRP are presented in Table 2.

The laser-machined microchannels are tapered due to the limitation of laser diffraction, as presented in Fig. 3(a). Therefore, the 1 mm CFRP or even thicker samples will not be cut through if single scanning path is applied. Although increasing the number of scanning times can improve the machining depth, which leads to HAZ increased and MRR reduced. In this investigation, a multiple path method is adopted in laser machining CFRP to reduce thermal damage and improve efficiency, as shown in Fig. 3(b). And the distance between the two paths is the laser scanning space h . The CFRP of the two tracks can gain more energy to remove the material which increases the MRR and reduces the HAZ.

2.2. Experiment setup

In this experiment, a 355 nm wavelength nanosecond Nd: YAG laser source was used for drilling CFRP, and the energy of laser beam is distributed as the Gaussian profile. In this laser system, the laser beam was moved in the x and y axis by the galvanometer mirror, and diameter of the laser beam spot is about 35 μm . The average laser power of 25 W and the frequency of 60 kHz were used for machining CFRP in this experiment, and the other specific processing parameters are shown in Table 1. Takahashi et al. [27] investigated the absorption of epoxy resin by an infrared laser and an ultraviolet laser. The epoxy resin hardly absorbs the infrared laser, while the UV laser can more effectively act on both the carbon fiber and the epoxy resin. So the 355 nm wavelength laser cutting CFRP can obtain better processing quality and processing efficiency [28]. The experimental procedure mainly includes 4 parts:

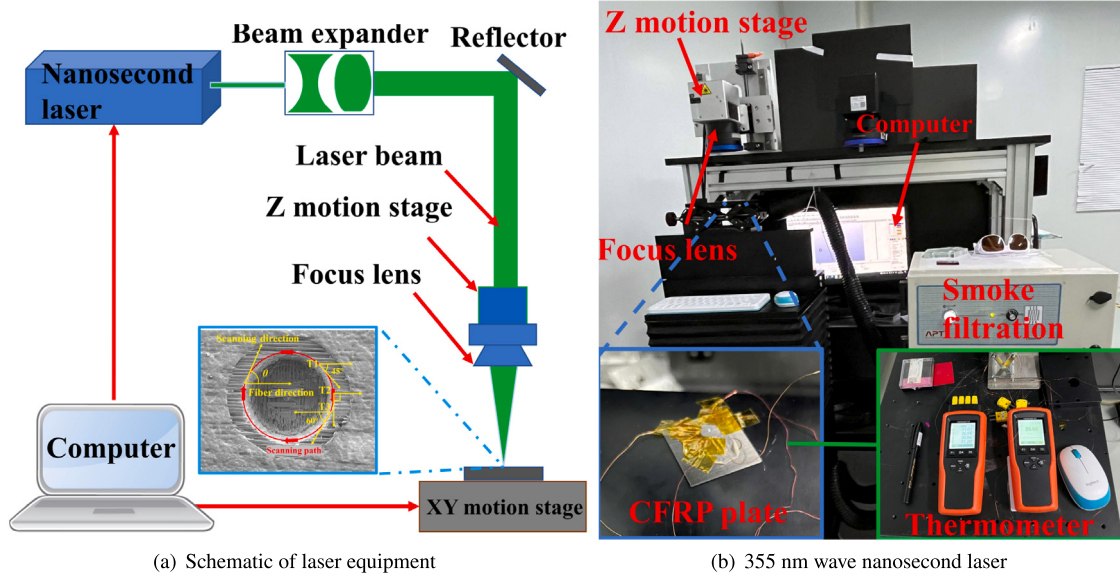


Fig. 1. Laser machining system.

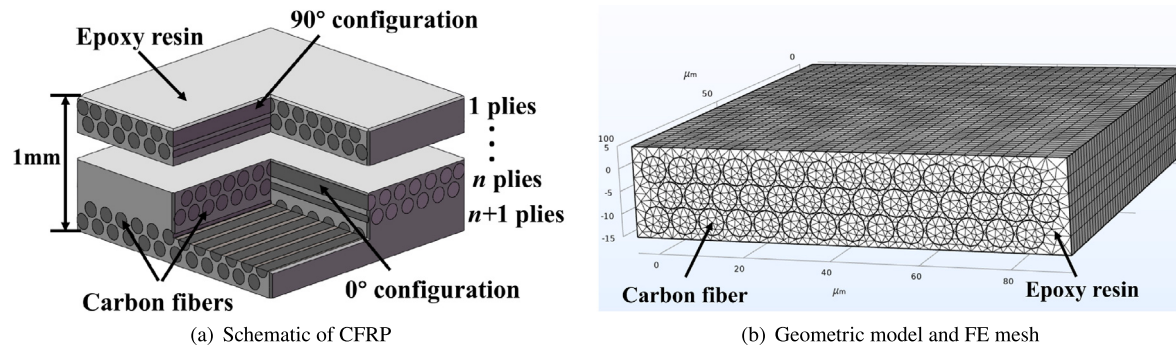
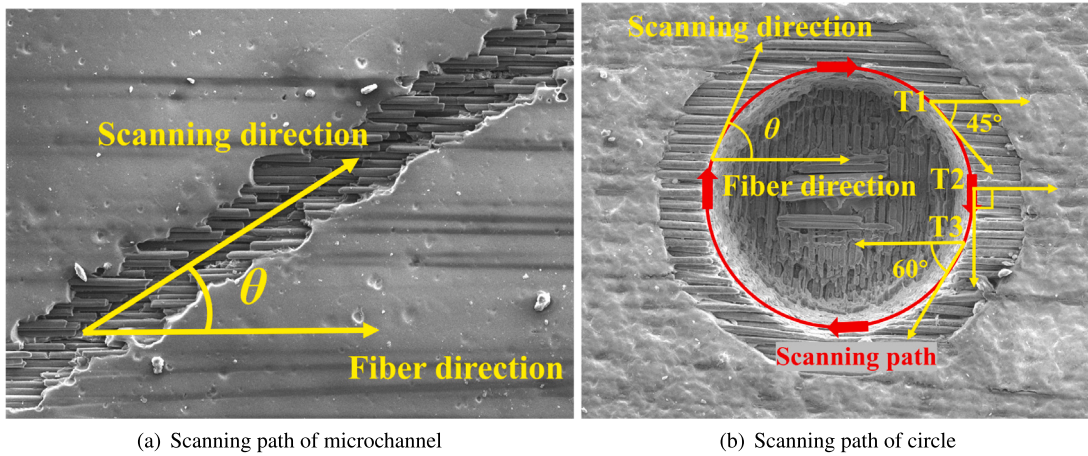


Fig. 2. Geometric model and schematic of CFRP.

Fig. 3. The angle θ between the scanning direction and fiber direction during laser processing.

straight-line processing (single laser scanning), circle processing (single laser scanning), micro-channel processing (*scanningtimes* = 45), and through-hole processing.

Firstly, a straight line with a length of 5 mm was processed on the CFRP with the laser, and the scanning time was 1. When laser processing holes in CFRP, the angle between the laser scanning direction and the carbon fiber direction varies continuously. Due to the anisotropic

heat transfer properties of carbon fibers, the scanning direction can affect the heat transfer of the carbon fibers, ultimately resulting in different levels of thermal damage and HAZ. So the angles between the laser scanning path and the carbon fiber are selected to study in this paper, including 0°, 30°, 45°, 60°, and 90°, as presented in Fig. 3. From Eq. (2), it can be seen that the overlap speed is decreasing as the laser scanning speed increasing, which in turn affects the processing

efficiency of the laser. Therefore, the laser scanning rate is used as a variable parameter in this study. The laser scanning speed is from 430 mm/s to 830 mm/s with an interval of 100 mm/s. The ablation morphology of CFRP and the fracture morphology of carbon fibers were observed by a field emission scanning electron microscope (SEM), and the average ablation depth and average ablation width of CFRP samples were measured by the laser scanning confocal microscope. Then the circles were machined with different laser scanning speeds (under single laser scanning), as shown in Fig. 3. The width of each circle was measured under different angles of 0°, 45°, and 90°, and compared with the experimental results of straight-line processing.

Then the microchannel machining experiment was carried out. Straight-line (single scanning) and micro-channel (multi scanning) were processed under the same laser scanning direction and laser scanning speed. Finally, the through holes with a diameter of 6 mm were processed by the method of concentric circles. SEM, EDX, and laser confocal microscope were used to observe the width and shape of the kerf, the oxidation degree of the processed area, and the width of the HAZ. According to the simulation results, the relationship between surface quality and scanning angles and scanning speeds were analyzed in detail.

2.3. Measurement/characterization

After the CFRP plates were processed, they were put into anhydrous ethanol with an ultrasonic cleaner for 5 min to wash away the processing debris and dust on the surface of the sample. Then the cleaned CFRP samples were placed in a dust-free environment to dry naturally. The ablation width, thermal damage, and kerf width of CFRP samples were observed by a field emission scanning electron microscope (SEM: JSM-7600F) produced by Japan Electronics Co., Ltd, and the resolution of the equipment is up to 1 nm. The distribution of C and O elements around kerf was observed by energy dispersive X-ray analysis (EDS). Different scanning angles θ and speeds v with different ablation depths, so the laser scanning confocal microscope (VK-X200K) produced by KEYENCE of Japan was applied to detect the micromorphology and ablation depth of CFRP samples. The width of thermal damage and depth of microchannel were measured three times, and the average value was obtained as the final result.

3. Numerical models

3.1. Geometric model and FE mesh

The CFRP plates have the characteristics of heterogeneity and anisotropy, in order to accurately describe the anisotropic heat transfer of laser processing CFRP, a heterogeneous geometric model is established by COMSOL Multiphysics software, as shown in Fig. 2. The axial thermal conductivity ($K_{yy} = 50 \text{ W/(m k)}$) of carbon fiber is higher than that of radial thermal conductivity ($K_{xx} = K_{zz} = 5 \text{ W/(m k)}$), the heat transfer heterogeneity of carbon fiber can be expressed by Eq. (1):

$$k = \begin{bmatrix} k_{xx} & k_{xy} & k_{xz} \\ k_{yx} & k_{yy} & k_{yz} \\ k_{zx} & k_{zy} & k_{zz} \end{bmatrix} \quad (1)$$

where K_{xx} represents thermal conductivity in the axial direction, K_{yy} and K_{zz} represent thermal conductivity in the radial direction.

Different heat transfer effects can be generated under the changing laser scanning direction due to the heterogeneity of heat transfer of CFRP, which ultimately results in different ablation morphology and HAZ. Fig. 4 shows the scanning direction θ and ablation morphology of the laser scanning. The relationship between the laser scanning directions and the removal mechanism of CFRP material was numerically analyzed under different scanning directions, so as to realize the purpose of explaining the mechanism of laser ablation of CFRP from microscopic level. In addition, pulsed laser machining is the result of

continuous ablation by multiple pulses, so the overlap rate of pulses will directly affect the width and depth of microchannel, as shown in Eq. (2) [29]:

$$I_P = 1 - \frac{v}{2rf} \quad (2)$$

where, v is the scanning speed, r is the radius of laser spot, and f is the repetition frequency of laser. The high laser scanning speed leads to the low overlap rate and the small processing depth and width of microchannel. Through the above analysis, the laser scanning direction and laser scanning speed have a great impact on the ablation results, so the simulation analysis is carried out to reveal the ablation mechanism of laser processing CFRP at a microscopic level.

3.2. Governing equations and boundary

(1) Governing equations

In this investigation, the energy of laser beam is distributed as the Gaussian profile, the laser power density as shown in Eq. (3)[30–32]:

$$q'' = \frac{2P}{\pi r^2} e^{\frac{(x-x_0-v_x t)^2+(y-y_0-v_y t)^2}{r^2}} \quad (3)$$

where P is the average power of laser, r is the radius of laser spot, x_0 is the horizontal coordinate of the laser spot center, y_0 is the vertical coordinate of the laser spot center. Different materials have different absorption rates of laser energy, so it is necessary to consider the absorption coefficient A of CFRP for laser energy, which is about 80% [30].

The angle between the laser scanning direction and the carbon fiber direction is θ . Different processing directions will lead to different heat transfer effects in the x and y axes, so v_x and v_y should be introduced into the heat source, as shown in Eqs. (4):

$$\begin{cases} v_x = v \cdot \sin\theta \\ v_y = v \cdot \cos\theta \end{cases} \quad (4)$$

Energy absorption coefficient A are introduced into Eq. (3), and combining Eq. (4), the governing equation of laser heat flux can be obtained, as shown in Eq. (5):

$$q'' = \frac{2PA}{\pi r^2} e^{\frac{(x-x_0-v_x t)^2+(y-y_0-v_y t)^2}{r^2}} \quad (5)$$

The heat transfer of nanosecond laser processing involves the law of energy conservation and fourier heat transfer law, as shown in Eqs. (6) and (7):

$$-\frac{\partial q''}{\partial n} + Q = PC \frac{\partial T}{\partial n} \quad (6)$$

$$q'' = -K(T) \frac{\partial T}{\partial n} \quad (7)$$

Combining Eqs. (6) and (7), the governing equation of heat conduction is obtained, as shown in Eq. (8):

$$(\Phi_p \rho_p C_p + \Phi_f \rho_f C_f) \frac{\partial T}{\partial t} = \frac{\partial}{\partial x} (k_{xx}(T) \frac{\partial T}{\partial x}) + \frac{\partial}{\partial y} (k_{yy}(T) \frac{\partial T}{\partial y}) + \frac{\partial}{\partial z} (k_{zz}(T) \frac{\partial T}{\partial z}) \quad (8)$$

where r_f and C_f are the density and specific heat capacity of carbon fiber, ρ_p and C_p are the density and specific heat capacity of the epoxy resin matrix.

Considering the latent heat L_f and L_p generated by carbon fiber evaporation and epoxy resin pyrolysis during laser processing, two source terms were introduced into final heat conduction equation, as shown in Eq. (9)[33]:

$$(\Phi_p \rho_p C_p + \Phi_f \rho_f C_f) \frac{\partial T}{\partial t} = \frac{\partial}{\partial x} (k_{xx}(T) \frac{\partial T}{\partial x}) + \frac{\partial}{\partial y} (k_{yy}(T) \frac{\partial T}{\partial y}) + \frac{\partial}{\partial z} (k_{zz}(T) \frac{\partial T}{\partial z}) - \Phi_p \rho_p L_1 \frac{\partial \alpha - 1}{\partial t} - \Phi_f \rho_f L_2 \quad (9)$$

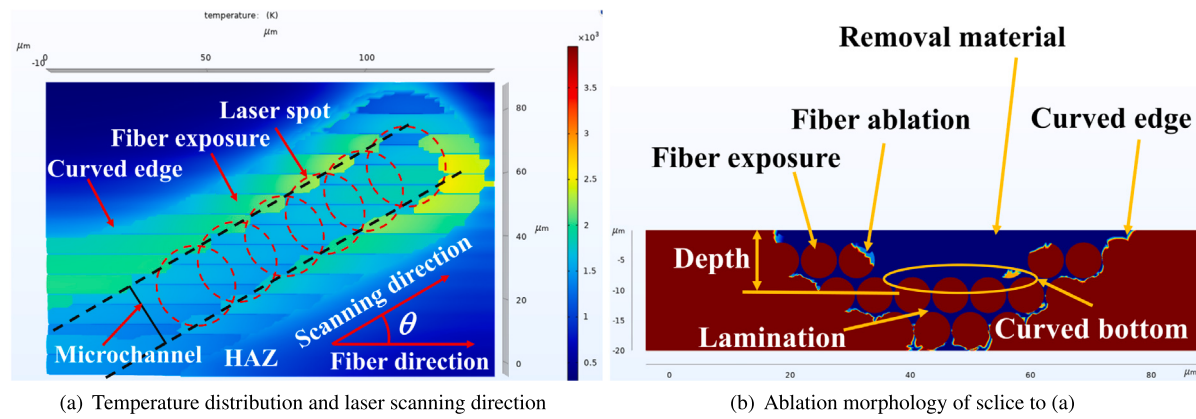


Fig. 4. Laser scanning direction and ablation morphology.

where α_p and α_f represent the decomposition rate of epoxy resin and carbon fiber.

The morphology and surface quality of the processed CFRP depend on the power density, which can be obtained from Eq. (10)[34]:

$$F = \frac{4P}{\pi d^2} \quad (10)$$

where P is the average power of the laser, and d is the diameter of the laser spot. Through the above analysis, the laser heat source is applied to the surface of the CFRP geometric model, and the laser moves along different scanning directions. The temperature generated inside the CFRP sample conforms to the heat transfer Eq. (10).

When the temperature reaches the vaporization threshold of carbon fiber or epoxy, the material will be removed, which can be expressed by (11):

$$T_{p,f} = \begin{cases} 0 & T < T_h \\ 1 & T > T_h \end{cases} \quad (11)$$

where $T_{p,f}$ represents the evaporation threshold of epoxy resin and carbon fiber. In the simulation, it is considered that all the corroded materials are converted into gas and will not participate in the subsequent simulation.

(2) Boundary conditions

In order to ensure the accuracy and uniqueness of the solution, boundary conditions should be set for the simulation model. The initial temperature of CFRP sample is 293.15 K, as shown in Eq. (12):

$$T(n, 0) = 293.15 \text{ K} \quad (12)$$

The boundary conditions of the upper surface of the sample include absorption of laser heat and heat convection with air, as shown in Eq. (13):

$$K(T) \frac{\partial T}{\partial n} = q''(1 - R) - h(T_0 - T) \quad (13)$$

where A is the laser absorption coefficient of CFRP, T_0 is the ambient temperature, and h is the convection heat transfer coefficient. The boundary condition of the side and bottom of the CFRP sample is heat convection with the air, as shown in Eq. (14):

$$K(T) \frac{\partial T}{\partial n} = -h(T_0 - T) \quad (14)$$

3.3. Assumptions

Laser ablation mechanism is a complex material removal process, including photodissociation, thermal ablation, and mechanical ablation. However, in the process of laser machining CFRP, the material is mainly removed by thermal corrosion. Therefore, only thermal corrosion removal is considered in the simulation of laser processing CFRP, and the following assumptions are made:

(a) Carbon fibers and resins are completely converted to gases when the temperatures reach the evaporation threshold;

(b) In the simulation, phase transformation is considered as the main corrosion mechanism, so the effects of photodissociation and mechanical corrosion are not considered.

3.4. Comparison with the previous simulation models

A comparison was made between this study and previous research about similar investigations, as shown in Table 3. Few researchers applied a homogenized geometric model considering anisotropic heat transfer to study the ablation mechanism and heat transfer of laser processing CFRP under different scanning directions. Although some heterogeneous geometric numerical models were established for numerical simulation analysis, the anisotropy of carbon fiber heat transfer and heat transfer under different scanning directions were not analyzed.

A homogenization numerical model was established to investigate the ablation depth of laser machining. But the isotropic model makes it impossible to simulate anisotropic heat transfer in laser processing [33]. Although a heterogeneous model was developed considering the differences in heat transfer between carbon fibers and epoxy resin, the effects of heat accumulation by multiple pulses, scanning direction, and anisotropy of carbon fibers on the ablation mechanism were not investigated [30]. In laser-processed CFRP, heat accumulation is a significant factor causing thermal damage and HAZ. Xu et al. [35] established a heterogeneous geometric model considering anisotropic heat transfer under different laser scanning directions, but the effect of multiple pulse heat accumulation on material removal and thermal damage formation was ignored, making it impossible to accurately reveal the ablation mechanism of laser processing CFRP. Ohkubo et al. [22] accurately revealed the difference in the removal speed of carbon fiber and resin by numerical analysis, while the effect of heat accumulation on the ablation mechanism was also ignored.

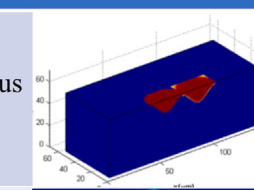
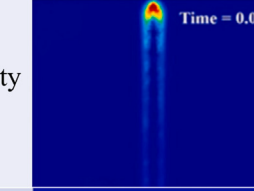
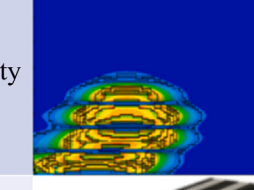
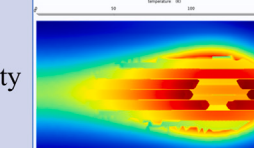
In this study, a model of laser processing heterogeneity CFRP was established, and the anisotropic heat transfer of carbon fibers during laser processing is considered based on numerical simulations. The combination of simulation and experimental studies reveals more precisely the mechanism of thermal damage and HAZ formation in laser ablation of CFRP.

4. Results and discussion

4.1. Heat transfer mechanism under different laser scanning directions

CFRP plate has the characteristics of heterogeneity and anisotropy, so the uneven heat transfer phenomenon occurs in laser processing CFRP, which leads to serious HAZ and thermal damage. The experimental results show that the laser scanning direction is one of the

Table 3
Comparison of models with the published article [22,30,33,35].

Author	Scanning direction	Heat transfer	Number of pulse	Numerical result	
Xu et al.[33]	Ignored	Isotropic heat transfer of CFRP	Two pulses	Homogeneous model	
Wang et al.[30]	0°	Isotropic heat transfer of carbon fiber	One pulse	Heterogeneity Model	
Xu et al.[35]	0°,15°, 30°,45°, 60°,75°, 90°	Isotropic heat transfer of carbon fiber	Two pulses	Heterogeneity Model	
Ohkubo et al. [22]	Ignored	Anisotropic heat transfer of carbon fiber	One pulse	Heterogeneity Model	
Current study	0°, 30°,45°, 60°, 90°	Anisotropic heat transfer of carbon fiber	Multiple pulses	Heterogeneity Model	

key factors affecting thermal damage and HAZ. Therefore, the ablation morphology and machining quality of laser processing CFRP were simulated under different scanning directions ($\theta = 0^\circ, 30^\circ, 45^\circ, 60^\circ, 90^\circ$) and scanning speeds ($v = 430 \text{ mm/s}, 530 \text{ mm/s}, 630 \text{ mm/s}, 730 \text{ mm/s}, 830 \text{ mm/s}$) in this study.

In order to reveal the ablation mechanism of laser processing CFRP under multiple pulses (9 pulses), the ablation process of CFRP was simulated and analyzed, which involved the distribution of temperature, ablation morphology, and HAZ. After 9 pulses laser was applied to CFRP, a microchannel with an irregular kerf and exposed fiber was obtained. There are two reasons for the above simulation results. On the one hand, the difference in evaporation threshold (as presented in Table 2) between carbon fiber and epoxy resin leads to the epoxy resin being easily removed because of its low evaporation temperature. On the other hand, epoxy resin has the characteristic of lower thermal conductivity than that of carbon fiber, so more heat is accumulated in epoxy resin. For the above two reasons, the epoxy resins are removed firstly while the carbon fiber still remains.

Furthermore, with the increase of scanning angle, the width of HAZ and the width of thermal damage go up gradually, and the width of thermal damage and HAZ go up under the scanning direction of $\theta = 90^\circ$, as shown in Fig. 5. There are two main reasons for this phenomenon. On one hand, the heat conductivity of the axial direction is 10 times the radial direction due to the heat transfer anisotropy of carbon fiber, according to Eq. (1), which results in serious heat transfer along the axis direction of the carbon fiber. The heat absorbed by the epoxy resin contributes to serious thermal damage and HAZ. On the

other hand, the energy of the laser is distributed by Gaussian, so the temperature at the laser spot central is the highest, and the temperature at the edge of the laser spot is the lowest. Although the laser energy at the edge of the laser spot is too low to remove the carbon fiber, it can easily ablate epoxy resin due to its low vaporization temperature. So there are many carbon fibers are exposed on both sides of the microchannel. Therefore, the ablation width of carbon fiber is larger, but the HAZ and thermal damage width are smaller under the scanning direction of 0°. When the laser scanning direction is 90°, the less carbon fiber is ablated, but serious thermal damage and HAZ are formed, which leads to the degradation of the epoxy resin.

The width of the microchannel decreases with the increase of the laser scanning speed, as shown in Fig. 5. The depth and width of ablation in laser machining CFRP are the largest under the scanning speed of 430 mm/s. But only a small amount of carbon fiber is eroded with serious thermal damage around the machining area with a scanning speed of 830 mm/s. In addition, the width of thermal damage decreases with the scanning speed going up, as shown in Fig. 5(c), (f), and (i). The pulse overlap rate is the main reason for the above phenomenon. According to Eq. (2), the pulse overlap rate decreases with the scanning speed, so the pulse overlap rate at the scanning speed of 430 mm/s is greater than that at the scanning speed of 830 mm/s. Therefore, the laser energy applied to the surface of CFRP is larger with a scanning speed of 430 mm/s, resulting in serious ablation.

The variation of ablation depth and width under different machining parameters in the simulation was presented in Fig. 6(a) and (b). It can be seen that the ablation width increases with the scanning

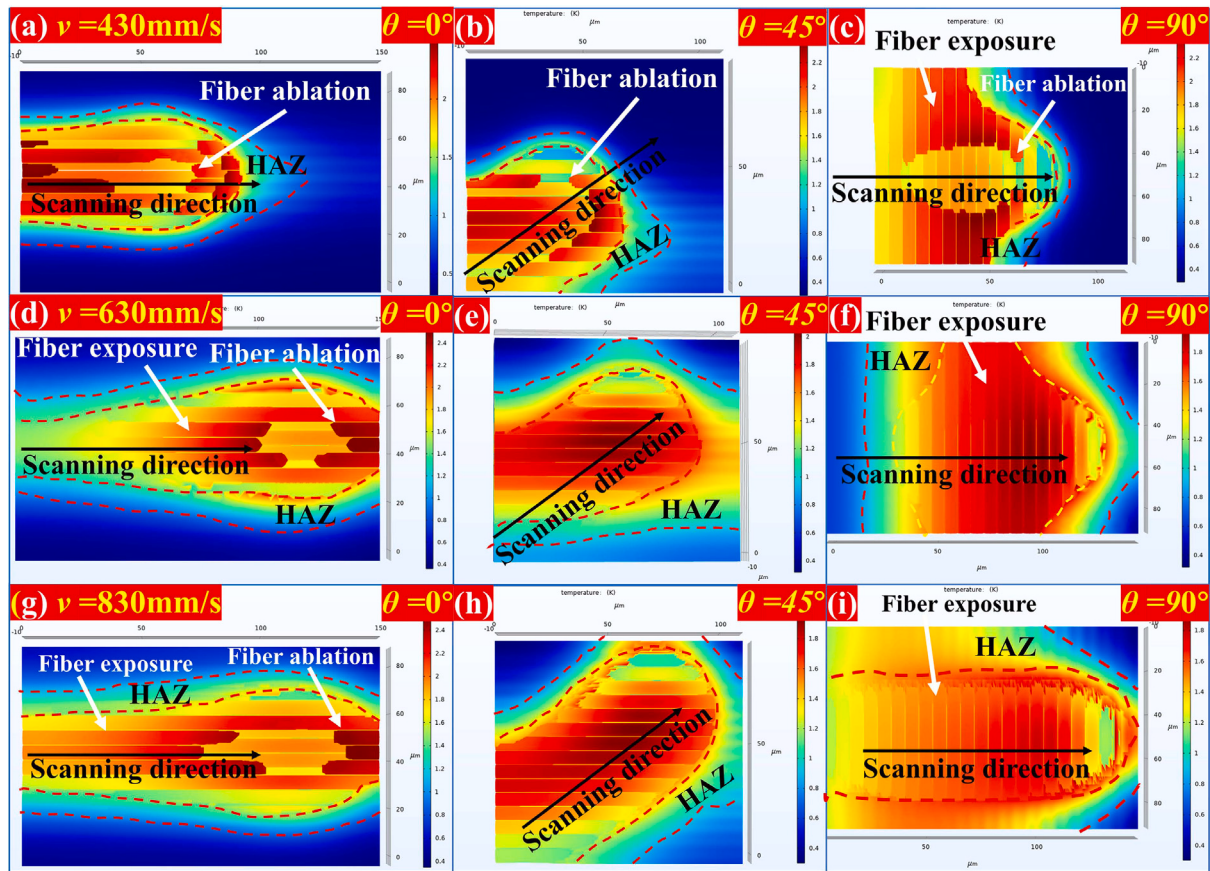


Fig. 5. Ablation morphology of microchannel under different scanning directions and speeds in simulation (single-scanning; $v = 430$ mm/s, 630 mm/s, 830 mm/s; $\theta = 0^\circ$, 45° , 90°).

direction angle θ increasing, but it decreases with the increasing of scanning speed. The minimum ablation depth is 38.27 μm , and the maximum ablation depth is 78.81 μm . When the scanning speed is 530 mm/s, a great change in ablation width is obtained under different machining directions, increasing by 73.94%. As shown in Fig. 6(b), the ablation depth decreases with the increase in the scanning angle and scanning speed. This is mainly because the increase in scanning speed leads to a decrease in pulse overlap rate, which finally leads to a decrease in ablation width and ablation depth. In addition, more laser energy is transferred along the axial direction of the carbon fiber to the surrounding epoxy resin as the scanning angle increases, which contributes to serious thermal damage. According to the law of energy conservation, too much laser energy is used to ablate the epoxy resin, leading to less laser energy in the ablation depth.

In order to verify the temperature distribution in the simulation, the temperature of laser machining an open hole was tested. The diameter of the hole is 6 mm, and temperature sensors are placed at 45° , 60° , and 90° on the circle with a diameter of $D = 6$ mm, 6.6 mm, 7.2 mm, and 7.8 mm respectively, as shown in Fig. 1(b). As shown in Fig. 7, the temperature decreases with the increase of scanning angle θ increasing. The main reason is the difference in heat conductivity between the axial direction (50 W/(m k)) and the radial direction (5 W/(m k)) of carbon fiber, as shown in Table 2. When the scanning direction θ is 90° , more laser energy is transferred along the axis of the carbon fiber, resulting in a lower temperature at the measuring point. But, more heat is accumulated with the scanning direction θ of 45° . For example, at the scanning direction of 90° , the temperature is lower than that under the scanning direction of 45° . In addition, it can be seen that the temperature decreases with the increase of diameter D . The energy of the laser conforms to the Gaussian distribution, and the temperature in the center of the laser spot is the highest and decreases with the

increase of laser spot diameter. Therefore, the temperature decreases gradually with the increase of diameter D when laser machining an open hole, as shown in Fig. 7. And the reason is that the temperature on both sides of the microchannel gradually decreases in the simulation, as shown in Fig. 5.

4.2. Ablation mechanism under different laser scanning directions

The CFRP microchannel was machined by nanosecond laser in the experiment (single-scanning) to verify the simulation, under scanning directions ($\theta = 0^\circ$, 30° , 45° , 60° , 90°) and scanning speeds (430 mm/s, 530 mm/s, 630 mm/s, 730 mm/s, 830 mm/s). The results of the experiment including ablation morphology and thermal damage of the CFRP microchannel are shown in Fig. 8. When the speed is 830 mm/s and the scanning direction is 0° , the minimum ablation width is obtained at 49.16 μm . The maximum ablation width is up to 102.84 μm under a scanning speed of 430 mm/s and a scanning direction of 90° .

Laser scanning speed is one of the key factors affecting the microchannel width, so the effect of the scanning speed on the microchannel width is investigated. As shown in Fig. 8, the microchannel width increases with the scanning angle θ increasing, but with less carbon fiber ablation. When the scanning directions are 0° , 30° , 45° , and 60° , many carbon fibers break and form micro-grooves. Compared with the results under the scanning direction of 90° , there is almost no carbon fiber eroded, but wider thermal damage is formed. This is mainly because more carbon fiber is irradiated by the laser beam with the scanning angle increasing, resulting in heat transfer along the carbon fiber to the surrounding epoxy resin and forming a wider ablation width. In addition, the ablation width decreases with the laser scanning speed, and the width ranges from 49.16 μm to 102.84 μm . This is mainly attributed to the laser pulse overlap rate according to Eq. (10). The

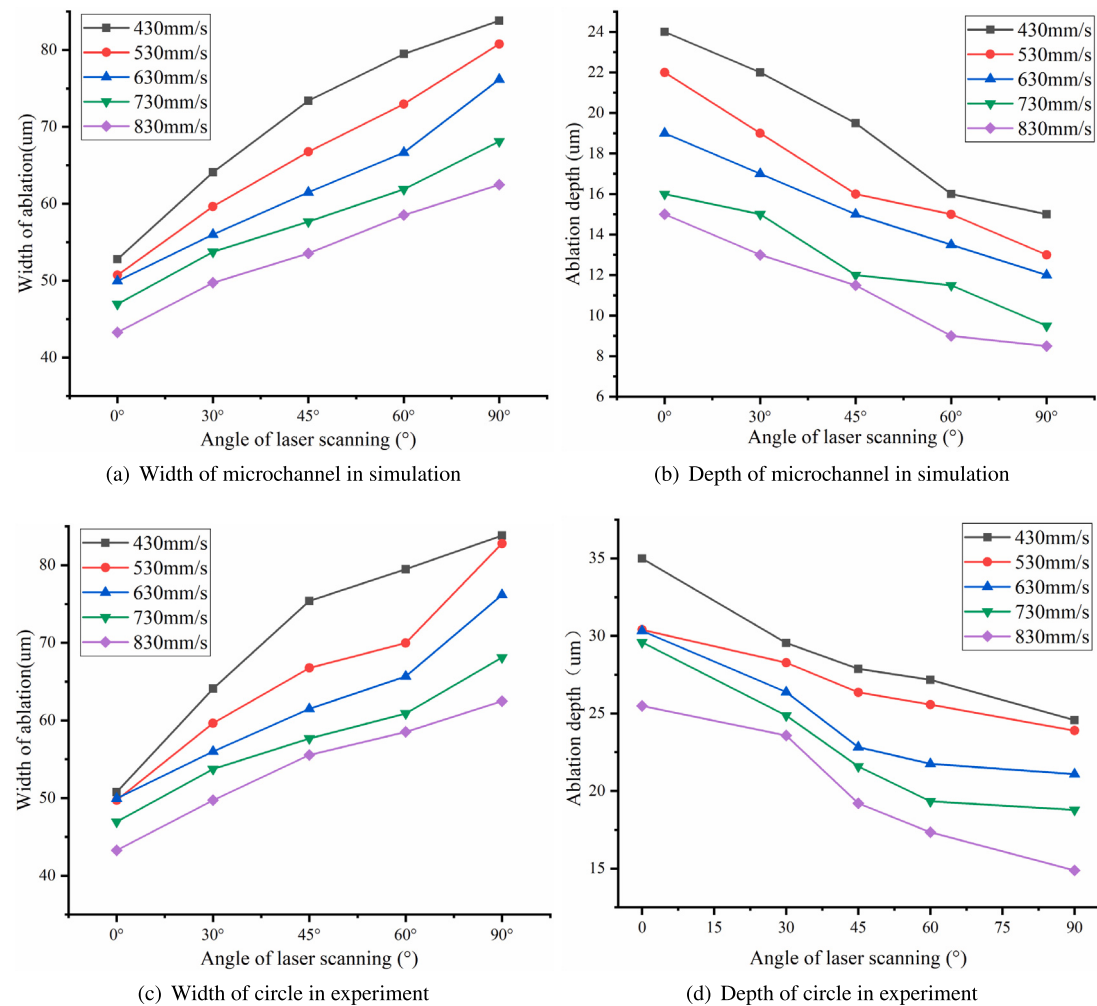


Fig. 6. Effect of scanning direction and speed on width and depth of microchannel in simulation and experiment (single-scanning).

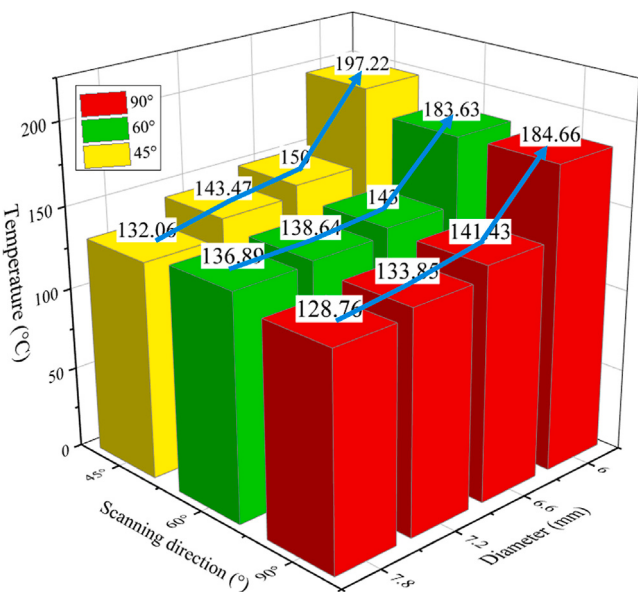


Fig. 7. Temperature distribution at different positions of the through-hole in experiment corresponding to Fig. 1(b).

higher the scanning speed, the lower energy per unit area applies on, which leads to a decrease in the microchannel width.

The variation of microchannel width under different machining parameters in the experiment is shown in Fig. 6(c). It can be seen from Fig. 6(c) that the microchannel width increases with the scanning direction θ , as shown in Fig. 6(c). The maximum microchannel width is about 102.84 μm , the minimum width is about 49.16 μm , and the maximum ablation width increased by 77.4% ($v = 430 \text{ mm/s}$). Through the above analysis, it is found that the ablation morphology and ablation width in the experiment are consistent with the simulation result, and the average deviation between experiment and simulation ranges from 5.01% to 16.99%. So the model established in this study could accurately reveal the mechanism of laser processing CFRP.

The variation of microchannel depth under different machining parameters in the experiment is shown in Fig. 6(d). The ablation depth decreases with the increase of the scanning angle increasing, as presented in Fig. 6(d). The maximum depth is about 34.99 μm , the minimum depth is about 14.8 μm , and the maximum ablation depth increases by 42.41%. Therefore, the efficiency of laser machining CFRP can be improved by optimizing the scanning directions and speeds, and the maximum efficiency can be increased by 42.4%. In addition, the variation trend of ablation width and ablation depth in the experiment conforms to that of simulation results.

The magnifications of ablation morphology corresponding to Fig. 8(a), (b), (c), and (d) were observed by SEM, as shown in Fig. 9. Many carbon fibers are eroded and formed relatively deep micro-grooves with a neat section of carbon fibers under a scanning speed of

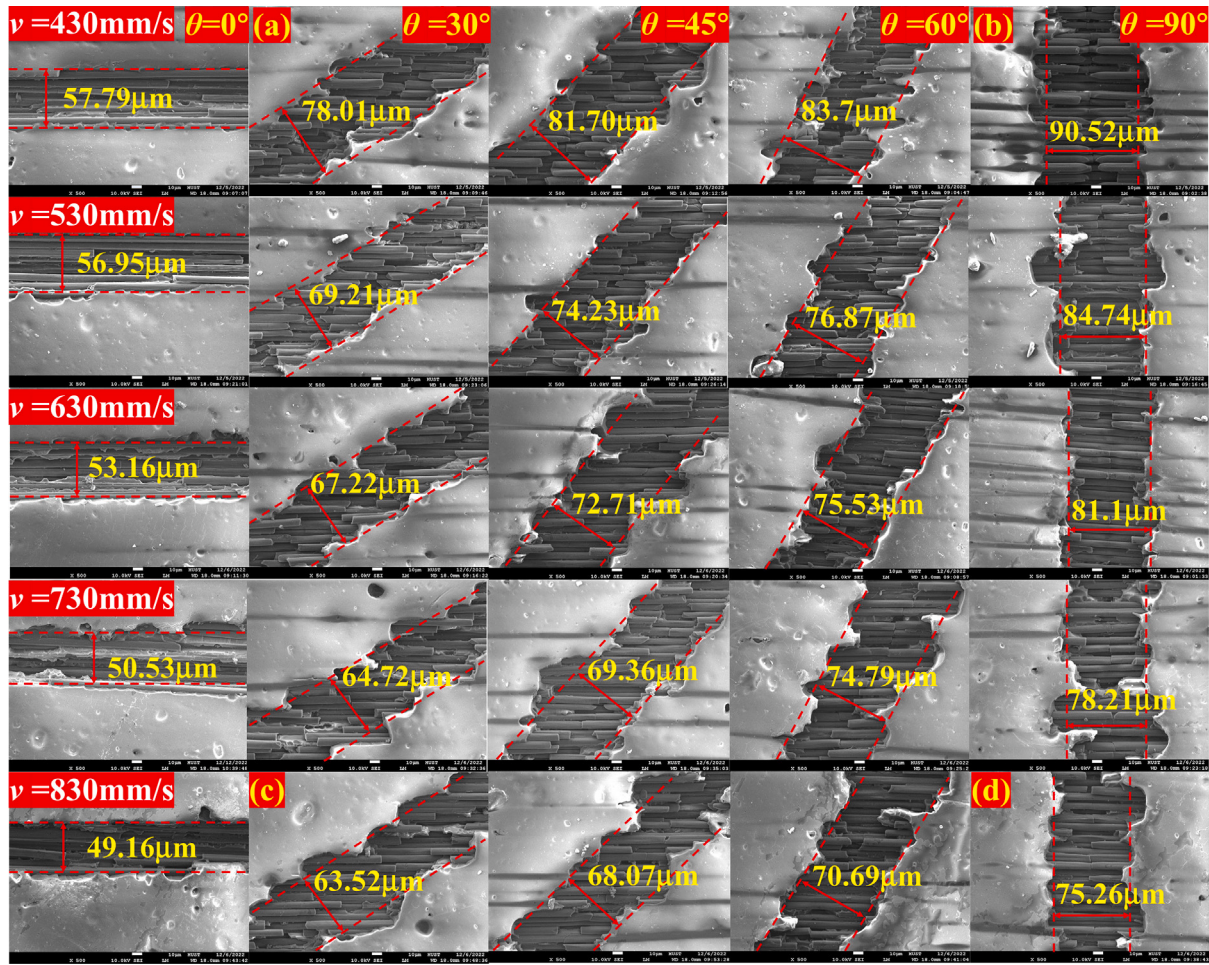


Fig. 8. Ablation morphology and width of microchannel under different scanning directions and speeds (single-scanning).

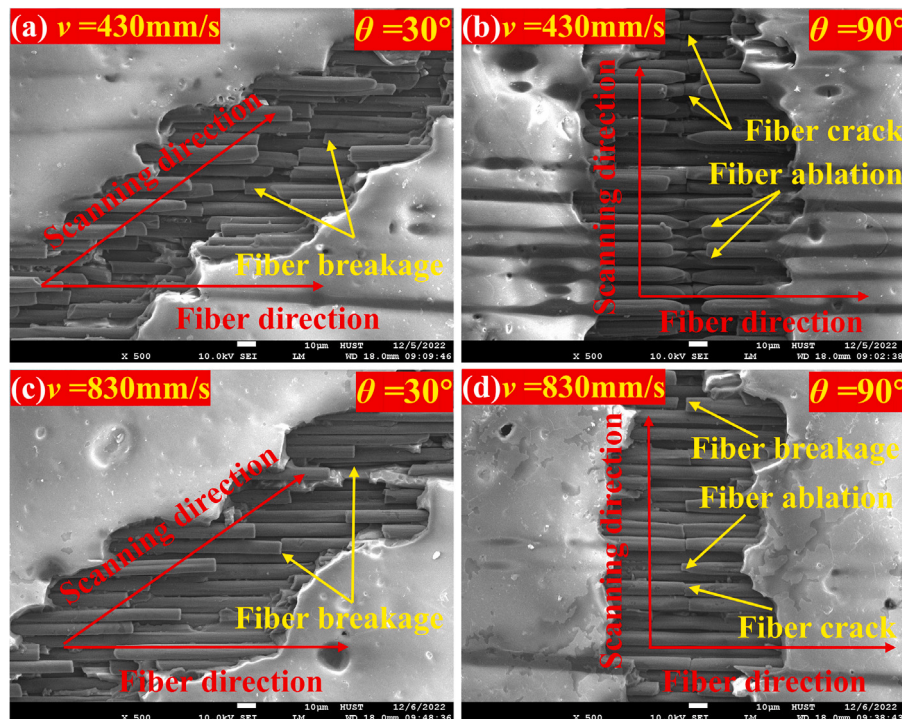


Fig. 9. SEM morphology of microchannel under different scanning directions and speeds corresponding to Fig. 8 (a), (b), (c), and (d).

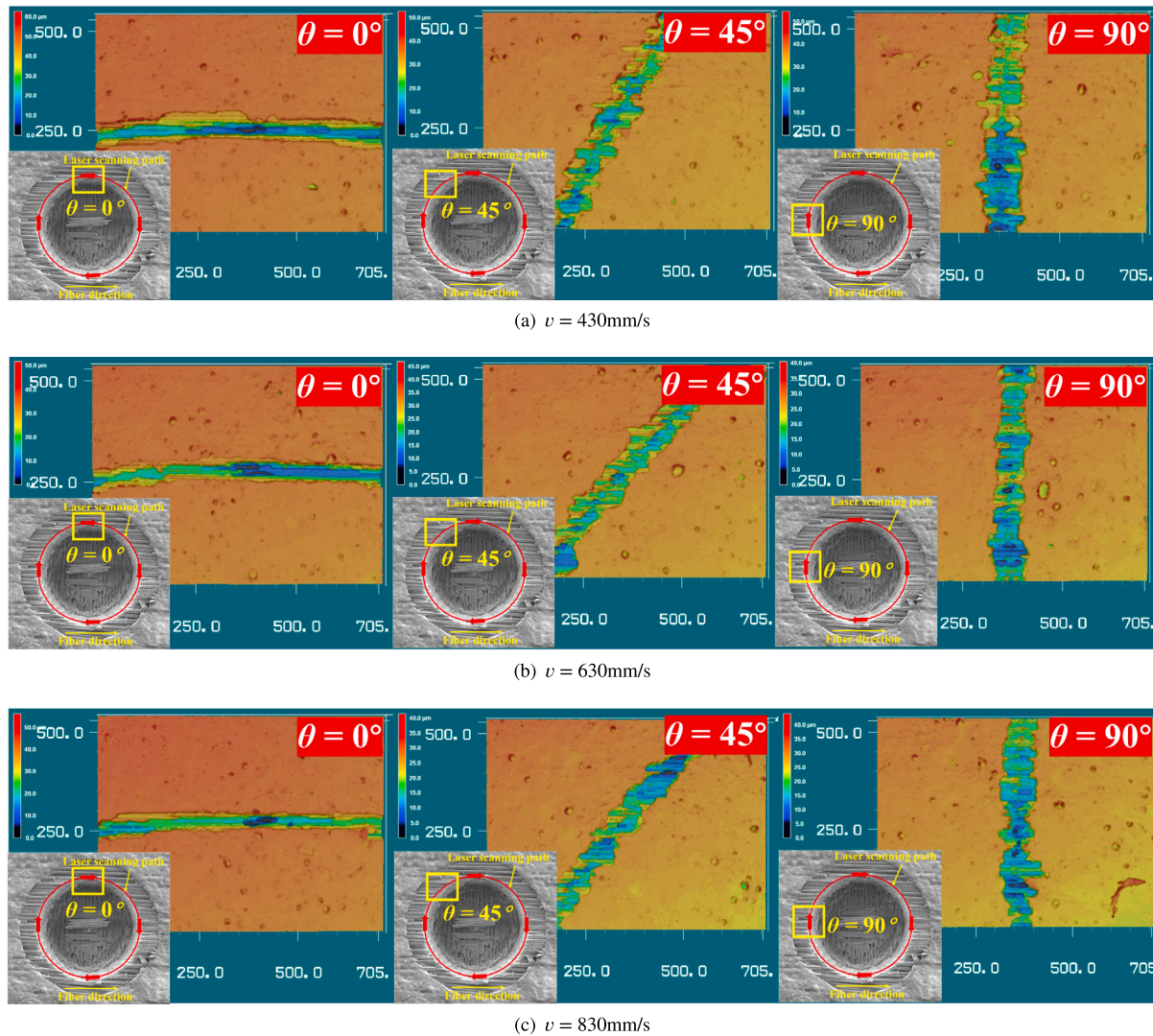


Fig. 10. 3D surface morphology of the circle under different laser scanning directions (single-scanning).

430 mm/s and a scanning direction of 30°, as shown in Fig. 9(a). This is mainly due to that the corrosion mechanism at this time includes thermal corrosion and mechanical corrosion, and mechanical corrosion is the main method of ablation. So the laser impact force breaks the carbon fiber forming a breakage section. In addition, a shallow microchannel with a conical section was machined by laser under the scanning direction of 90°, as shown in Fig. 9(b). This is due to thermal corrosion as the main method of ablation at this time, so a conical section is obtained. Fig. 9(c) and (d) show the machining results with a scanning speed of 830 mm/s. It can be seen from Fig. 9(c) that the number of broken carbon fibers is about 11, which is significantly reduced compared with Fig. 9(a). Besides, there are only a few carbon fibers removed with a scanning speed of 830 mm/s and a scanning direction of 90°, as presented in Fig. 9. This is mainly because the pulse overlap rate decreases with the scanning speed increasing, which in turn leads to a decrease in the energy applied to the CFRP material, ultimately leading to less material removed.

The angle between the laser scanning path and the direction of carbon fiber is constantly changing when laser process a circle on CFRP, as shown in Fig. 3. So the thermal damage, ablation width, and depth of the circle at different positions are different. The circles with a diameter of 6 mm were processed by laser under the scanning speeds of 430 mm/s, 630 mm/s, and 830 mm/s, respectively. A laser confocal microscope was used to observe the circle morphology at positions of

0°, 45°, and 90°, as shown in Fig. 10. The kerf is irregular and jagged under the scanning direction of 45° and 90°, but the kerf is relatively neat under the scanning direction of 0°. Because the carbon fiber in CFRP has the characteristic of anisotropic, the thermal conductivity of the axial direction is much higher than the thermal conductivity of radial direction. When the scanning direction is at 0°, the laser scanning direction is the same direction as the carbon fiber and kerf. Therefore, the energy of laser is transferred along the axial direction of the same bundle of carbon fiber, and the erosion edge of the surrounding epoxy resin is basically consistent with the direction of carbon fiber, presenting a relatively neat edge. When the scanning direction is at 90°, it is perpendicular to the direction of the carbon fiber. The heat is transferred along the carbon fiber and ablates the epoxy resin around it. Due to the uneven thickness of the epoxy resin, the large thickness of the epoxy resin is not completely removed, while the small thickness of the epoxy resin formed a large corrosion. As a result, the kerf appears jagged, as shown in Fig. 10.

It can be found that the ablation width of the circle is smallest at the position of 0° and increases with the scanning angle increasing. In addition, the ablation width decreases with the scanning speed declining, as presented in Fig. 11(a). When the laser scanning speed is 430 mm/s, the ablation width is the minimum; when the laser scanning speed is 830 mm/s, the ablation width of the circle is the maximum, as shown in Fig. 10. This is mainly due to the anisotropic

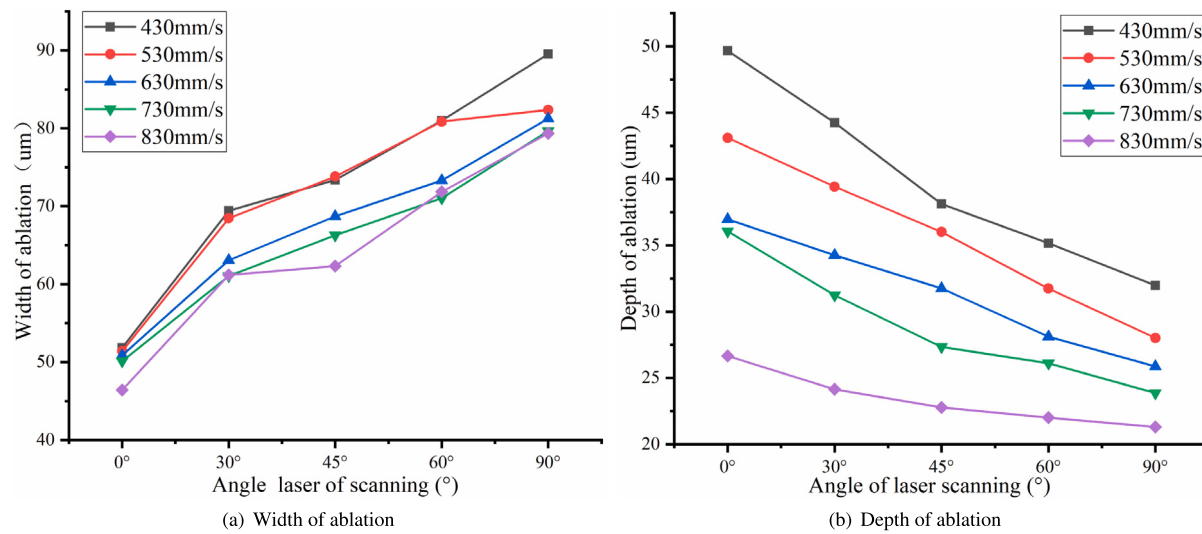


Fig. 11. Effect of processing parameters on ablation width and depth of circle (single-scanning).

heat transfer of carbon fiber. The width variation trend is the same as that of laser machining microchannel. Therefore, the main reason for this phenomenon is that the scanning speed affects the overlap of laser pulses; the lower the laser scanning speed, the higher the overlap and the energy density, so the greater the depth and width of the ablation obtained. Through the above analysis, the changing trend of ablation width conforms to that of the width of circle, that is, the ablation width increases with the scanning angle θ increasing, and the ablation width decreases with the increase of scanning speed, as shown in Fig. 11(a). According to Eq. (1), the axial thermal conductivity and radial thermal conductivity of carbon fiber are different, $K_{xx} = 50 \text{ W}/(\text{m k})$ and $K_{yy} = K_{zz} = 5 \text{ W}/(\text{m k})$. So the axial thermal conductivity is higher, which is 10 times the thermal conductivity of the carbon fiber radial direction. When the angle between the scanning direction and the carbon fiber direction is 90°, the laser beam is fed perpendicular to the direction of the carbon fiber, so the heat is transferred to the surrounding epoxy resin along the direction of the carbon fiber, resulting in the smallest ablation depth and the largest thermal damage width; when the angle between the scanning direction and the carbon fiber direction is 0°, the laser beam is fed along the direction of the carbon fiber, which leads to the heat accumulated on the carbon fiber and finally forms the processing effect of large ablation depth and small thermal damage width. Therefore, the processing depth decreases with the increase of the angle between the scanning direction and the carbon fiber direction when processing the circle.

The variation of ablation depth and width of the CFRP circles under different laser processing parameters were analyzed. It can be seen from Fig. 11(a) that the minimum ablation width is 46.42 μm ($v = 830 \text{ mm/s}$, $\theta = 0^\circ$) and the maximum ablation width is 89.53 μm ($v = 430 \text{ mm/s}$, $\theta = 90^\circ$), and the ablation width increases by 92.87%. In the low scanning angle, as the increase of laser scanning angle, more laser energy is transferred to the surrounding epoxy matrix along the axial direction of the carbon fiber, leading more epoxy to be removed sharply. Under the same laser scanning speed, the width of ablation significantly increases with the rise of the scanning angle. Therefore, more epoxy matrix in the width is decomposed, which improves the width of the microchannel. The minimum ablation depth is 21.31 μm ($v = 830 \text{ mm/s}$, $\theta = 90^\circ$) and the maximum ablation depth is 49.67 μm ($v = 430 \text{ mm/s}$, $\theta = 0^\circ$), as presented in Fig. 11(b). When the scanning speed is 430 mm/s, the ablation depth increases by 55.36% as the scanning angle increasing. The angle between the laser scanning direction and the carbon fiber direction becomes smaller, leading to a large amount of laser energy accumulated. Under the same laser scanning speed, the depth of ablation significantly decreases with the rise of the scanning angle. Therefore,

Table 4

Width of microchannel under different processing parameters according to Fig. 12 (Unit: μm).

Samples	0°	30°	45°	60°	90°
430 mm/s	62.63	52.15	39.40	36.49	35.26
530 mm/s	60.53	48.03	36.41	33.88	32.98
630 mm/s	52.81	42.70	33.87	33.13	31.23
730 mm/s	50.70	41.59	32.88	31.78	30.18
830 mm/s	46.32	38.96	31.36	31.07	29.65

more material in the depth is removed, which improves the depth of ablation. Variation trend of circle depth and width (Fig. 11) conforms to that of microchannel depth (Fig. 6). Through the above analysis, it can be concluded that the processing efficiency can be increased by 55.36% under the scanning direction θ of 0°.

4.3. Thermal damage and HAZ of microchannel under multi-scanning

CFRP is usually cut using a multi-scanning method to ensure that the material can be cut through (mentioned in Section 4.2). Therefore, different scanning directions and scanning speeds of the laser will affect the width of the kerf, thermal damage, and efficiency. The morphology, thermal damage, and HAZ of the microchannel under different laser scanning speeds ($v = 430 \text{ mm/s}$, 530 mm/s, 630 mm/s, 730 mm/s, 830 mm/s), and different scanning directions ($\theta = 0^\circ$, 30°, 45°, 60°, 90°) were detected by SEM, as presented in Fig. 12. It can be seen that the width of the microchannel decreases with the increase of the laser scanning angle, and the width reaches the maximum of 62.63 μm under the scanning direction of $\theta = 0^\circ$. When the scanning direction θ is 90°, the ablation width is a minimum of 29.65 μm, as shown in the Table 4. This is same as the width variation trend of the microchannel (single-scanning) in Section 4.2. In the same way, the width variation trend of the microchannel ($scanningtimes = 45$) is mainly caused by the anisotropic heat transfer of carbon fiber. And the radial thermal conductivity of carbon fibers is much higher than that of the resin matrix, so the laser energy is transferred and accumulated to the epoxy resin through the carbon fiber. When the scanning direction is 90°, the kerf direction is perpendicular to the carbon fiber direction, which leads to more laser energy transferred along the axial direction of the carbon fiber to both sides of the kerf. Therefore, more epoxy resin is ablated, which leads to a wider kerf. When the scanning direction is 0°, the laser scanning direction, the incision direction, and the carbon fiber direction are the same, which leads to more heat transferred along the axis of

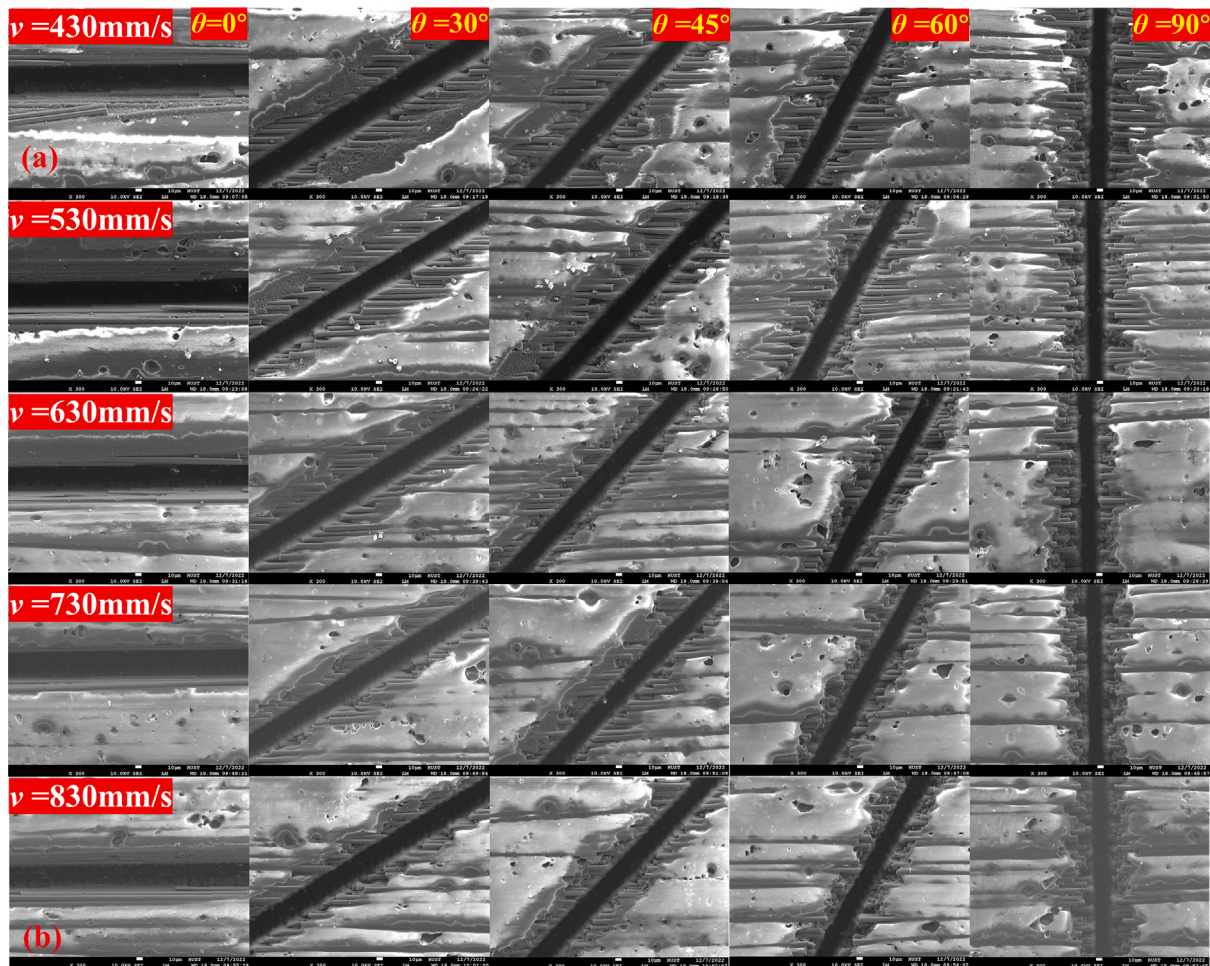


Fig. 12. SEM morphology of microchannel under different directions and speeds (scanning times = 45).

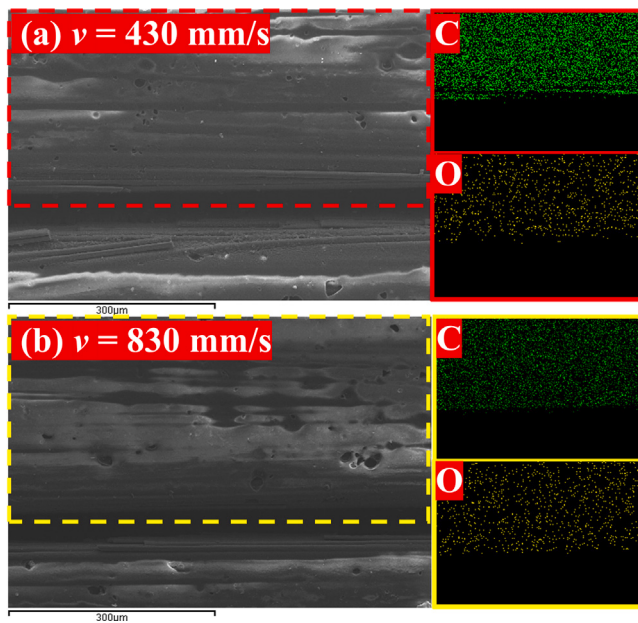


Fig. 13. SEM image and element distributions around the HAZ corresponding to Fig. 12 (a) and (b).

the carbon fiber. And only a little heat is transferred radially through carbon fiber to epoxy resin on the kerf, which reduces the width of the microchannel. Therefore, when the scanning direction is 0°, the ablation width is the smallest, which conforms to the variation trend of single-line microchannel width in Section 4.2. In addition, the width of the microchannel increase with the increasing of the scanning speed. And the pulse overlap rate decreases with the increasing of scanning speed, which reduces the energy density, and eventually decreases the ablation width.

What is more, it is found that the kerf under scanning directions of 0°, 30°, and 45° is relatively neat, and the edge of the epoxy resin is also smooth, as exhibited in Fig. 12. However, when scanning angles are 60° and 90°, the edges of the epoxy resin are jagged. This is contributed to the above reasons that more heat is transferred along the axial direction of the carbon fiber to the epoxy resin under the scanning direction of 60° and 90°, so the epoxy resin around the carbon fiber is eroded and forming a jagged edge.

In order to further analyze the influence of scanning speed on HAZ of the microchannel, SEM energy dispersive X-ray analysis (SEM-EDX) analysis was performed on element distribution around the HAZ of microchannel corresponding to Fig. 12 (a) and (b). The exposure of carbon fiber in HAZ results in an increase in the density of element C. As shown in Fig. 13, the density of the C element is obviously higher under the scanning speed of 430 mm/s than that under the scanning speed of 830 mm/s. This is mainly because the overlap of laser pulses increases when the scanning speed is lower, which leads to serious heat accumulation in CFRP. In the low laser scanning speed, the laser overlap rate goes up. So the time of laser irradiation the

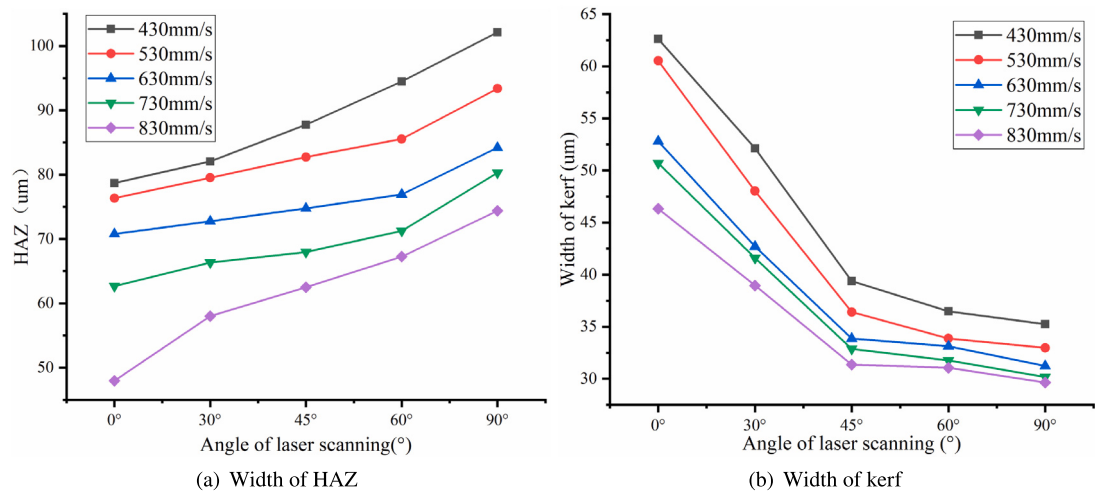


Fig. 14. Effect of processing parameters on HAZ width and kerf width of microchannel (scanning times = 45).

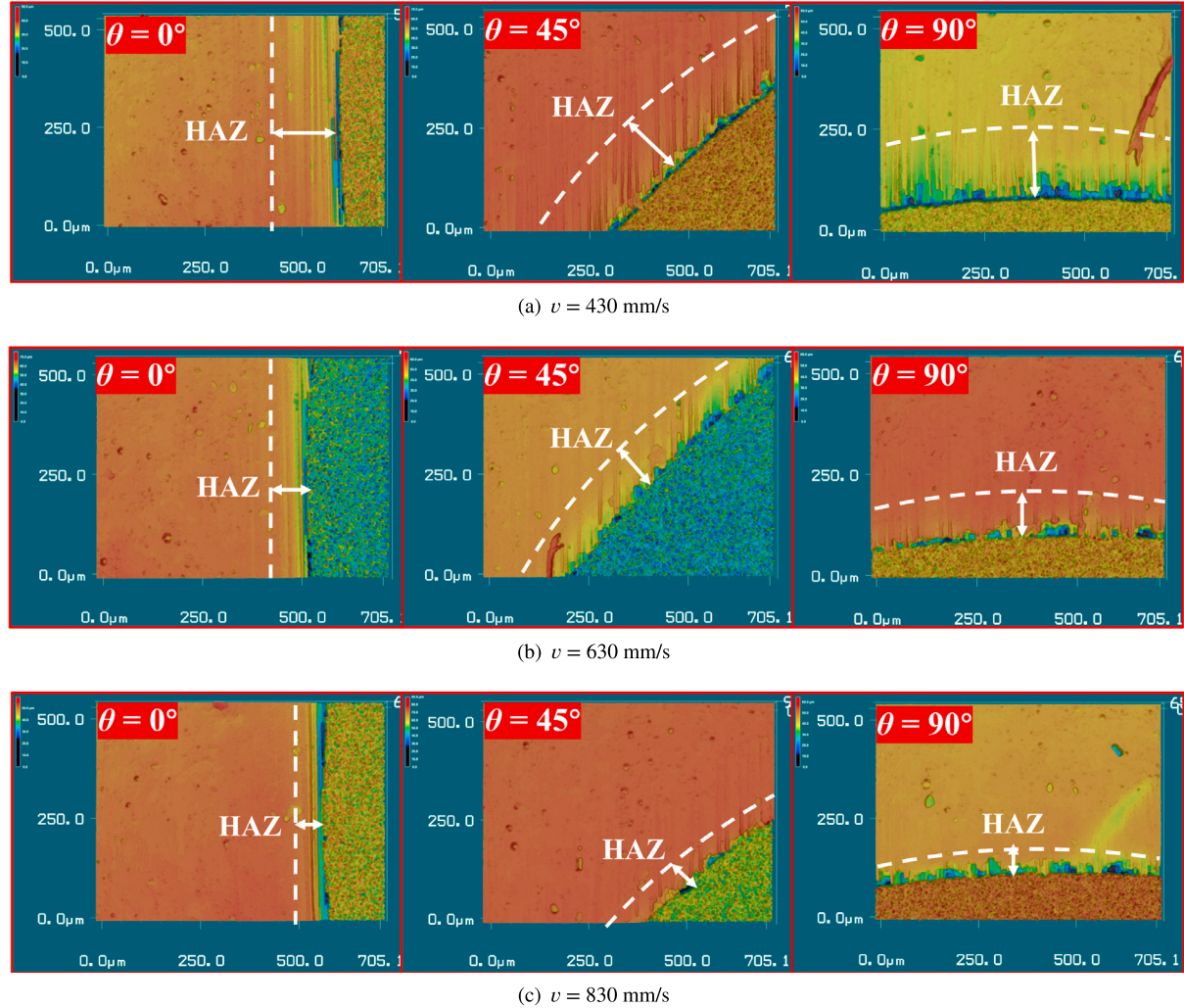


Fig. 15. 3D surface morphology of through hole under different processing parameters.

material becomes longer, which leads to more epoxy being oxidized or decomposed. As a result, the epoxy resin is decomposed and carbon fiber is exposed. So, the result shows that the thermal effect of the microchannel under speed of 430 mm/s is greater than that under scanning speed of 830 mm/s, which leads to serious decomposition of

epoxy resin. Through the above analysis, it can be further explained that with the increase of scanning speed, the HAZ and thermal damage become serious, as shown in Fig. 12.

The effects of laser scanning speed and scanning directions on microchannel quality was investigated, and the variation of kerf width and

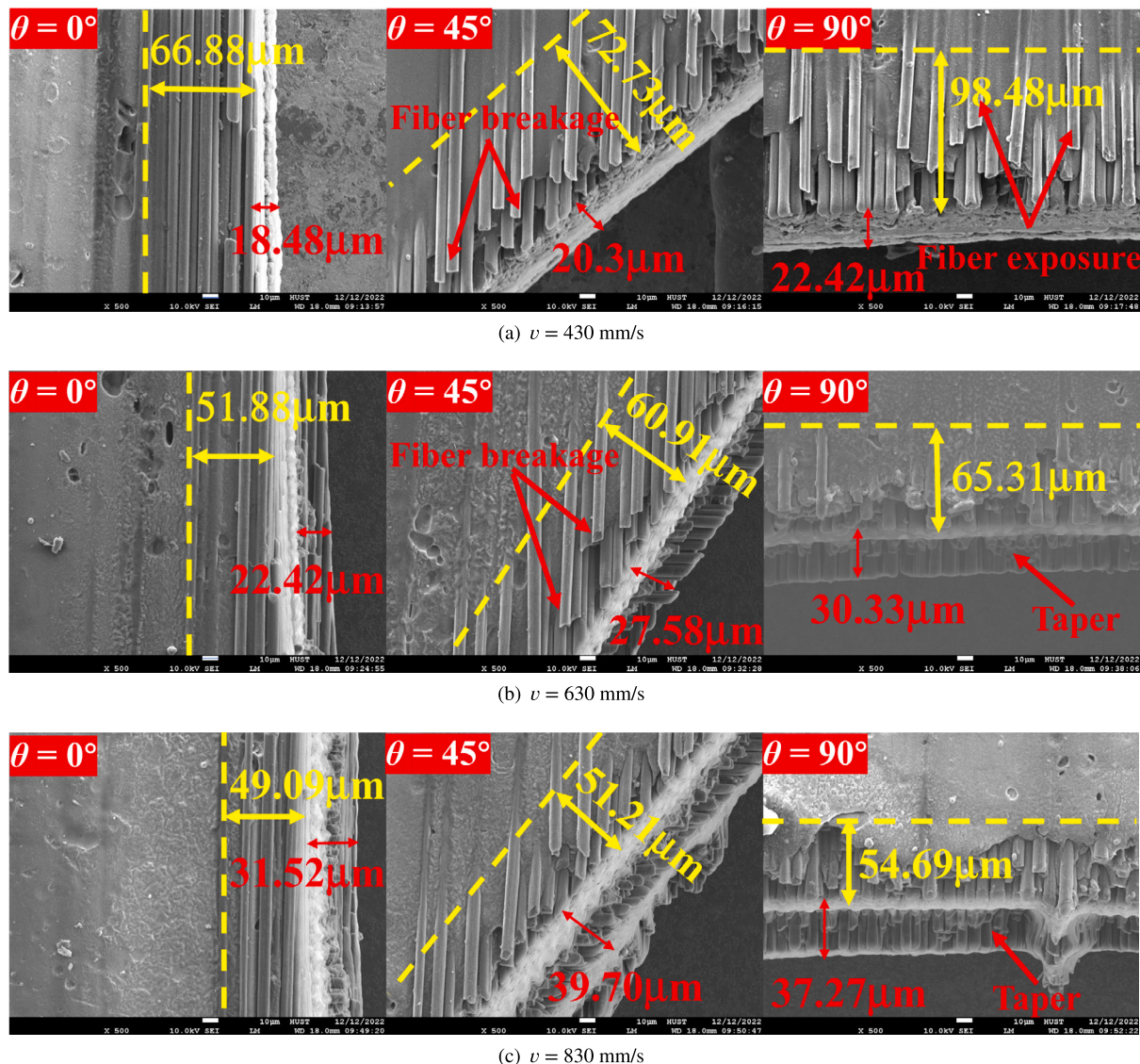


Fig. 16. Ablation morphology of through hole under different processing parameters.

depth under different machining parameters corresponding to Fig. 12 were analyzed, as shown in Fig. 14. It can be seen that the minimum HAZ width is 47.96 μm ($v = 830 \text{ mm/s}$, $\theta = 0^\circ$) and the maximum HAZ width is 102.12 μm ($v = 430 \text{ mm/s}$, $\theta = 90^\circ$). When the scanning speed is 830 mm/s, the width of HAZ decreases by 55.01% as the scanning direction decreases, as shown in Fig. 14(a). Therefore, the thermal damage width will be effectively reduced under the scanning direction of 0° . The minimum kerf width is 29.65 μm ($v = 830 \text{ mm/s}$, $\theta = 90^\circ$), and the maximum kerf width is 62.63 μm ($v = 430 \text{ mm/s}$, $\theta = 0^\circ$), as presented in Fig. 14(b). When the scanning speed v is 530 mm/s, the ablation width decreases by 83.53% with the increase of scanning angle. With the increase of laser scanning angle, laser energy is applied to more carbon fibers, which leads to heat transferring to the surrounding epoxy matrix and forming serious HAZ. Moreover, as the increase of the angle of laser scanning, more energy is used to ablate the epoxy resin and to increase the HAZ. According to the law of conservation of energy, less energy is used to remove the CFRP material in the depth direction. So under the same laser scanning speed, the HAZ becomes serious with the increase of the scanning angle, while the ablation depth decrease with the rise of the laser scanning angle. Through the above analysis, it can be concluded that the width of HAZ

is reduced by 55.01% under the scanning direction of 0° compared to that under the scanning direction of 90° , which can effectively improve the quality of laser processing CFRP.

4.4. Thermal damage and HAZ of through hole

The open holes are obtained by laser multi-scanning the circle (mentioned in Section 4.2). The angle between the laser scanning direction and the direction of carbon fiber is constantly changed during laser machining holes. So the thermal damage width, the exposure degree of carbon fiber, and the taper are different at different positions. The open holes with a diameter of 6 mm were drilled by laser under different scanning speeds (430 mm/s, 530 mm/s, 630 mm/s, 730 mm/s, 830 mm/s), and the machining quality at different positions (0° , 45° , 90°) was studied.

The thermal damage and HAZ of the open hole under different scanning speeds are shown in Fig. 15. From the image, it can be clearly seen that many carbon fibers were exposed at the edge of the kerf. The reasons for this phenomenon have been explained in Section 4.1, mainly because the energy of the laser is transferred along the axial direction of carbon fiber (due to the high axial heat conductivity); so

the epoxy resin around the carbon fiber is eroded, resulting in the carbon fiber exposed. Besides, the HAZ of the open hole decreases with the increase of scanning speed, as shown in Fig. 15. The width of HAZ is the maximum under the scanning speed of 430 mm/s, and the minimum under the scanning speed of 830 mm/s. Since heat accumulation decreases with the increase in scanning speed, reducing the width of the HAZ of the microchannel. By comparing with Fig. 14(a), it is discovered that the HAZ of the open hole and the HAZ of the microchannel have the same width variation trend, further demonstrating the validity of the relationship between scanning angle, scanning speed, and HAZ. Therefore, when laser processing CFRP through holes, the thermal damage and HAZ can be reduced under a higher processing speed, which reduces the decomposition of epoxy resin.

The surface morphology of the CFRP hole including thermal damage, exposed fiber, and taper was detected by SEM, as presented in Fig. 16. The thermal damage width increases with the increase of scanning angle θ , but decreases with the increase of scanning speed, which conforms to that of Section 4.3. In addition, the experimental results show that the angle of 0° has the smallest taper, but the angle of 90° has the largest taper. The taper is expressed by Eq. (15)[36]:

$$T = \frac{D_1 - D_2}{H} \times 100\% \quad (15)$$

where H is the thickness of the CFRP, D_1 , and D_2 are the diameters of the through holes on the upper and lower respectively. According to Eq. (15), when the scanning speed is 430 mm/s, the taper of the through hole is about 1.85%–2.24%, and the thermal damage width is 66.88 μm –98.48 μm . The taper of the through hole is 2.24%–3.03% when the scanning speed is 630 mm/s, and the thermal damage width is 51.88 μm –65.31 μm . When the scanning speed is 830 mm/s, the taper of hole is 3.15%–3.73%, and the thermal damage width is 49.09 μm –54.69 μm . Considering the width of thermal damage and the taper of CFRP holes, an optimized laser scanning speed of 630 mm/s is used to obtain the open hole with minimal HAZ and thermal damage.

The elliptical hole was formed by laser drilling due to the anisotropy of the CFRP plates [37]. The laser scanning direction is constantly changing with the direction of the carbon fiber, which leads to the constant change of heat transfer process in CFRP. When the angle between the scanning direction and the carbon fiber direction is 90°, the heat is transferred to the surrounding epoxy resin along the direction of the carbon fiber, resulting in the largest thermal damage width; when the angle between the scanning direction and the carbon fiber direction is 0°, the laser beam is fed along the direction of the carbon fiber, which leads to the heat accumulated on the carbon fiber and small thermal damage. Therefore, the elliptical hole formation due to the heterogeneity and anisotropy of the CFRP plates is a big challenge in laser drilling holes.

5. Conclusions

Nanosecond pulsed laser processing of CFRPs under different scanning directions was studied. Simulation and experiments were conducted to investigate the effect of scanning direction and speed on taper, HAZ, and thermal damage, which demonstrated the ablation mechanism. Based on the above results, the following conclusions were obtained:

(1) In this investigation, a model for nanosecond laser processing CFRP under different scanning directions was established considering heterogeneity and anisotropy. By comparison of simulation and experimental results, the deviation between simulation and experimental ranges from 5.01% to 16.99%.

(2) The ablation depth, ablation width, and HAZ of CFRP machined by laser under different process parameters were investigated. With the increase of the scanning angle, the width of HAZ goes up. CFRP machined by laser under a scanning direction of 0°, the ablation depth increases by 55.36%, and the ablation width decrease by 55.01% compared to that under the scanning direction of 90°.

(3) The taper of open hole decreases with the increase of the laser scanning speed. The pulse overlap decrease with the increase of the scanning speed, leading to some materials on the processed wall not being ablated forming a large taper.

(4) Thermal damage increases with the scanning speed decrease due to serious heat accumulation. A 355 nm wavelength nanosecond laser drilling under the scanning speed of 630 mm/s can obtain an excellent open hole with small HAZ and thermal damage. With the scanning speed increasing, the taper of the open hole ranges from 1.85% to 3.73%, while the thermal damage width ranges from 98.48 μm to 49.09 μm .

CRediT authorship contribution statement

Peng Wang: Formal analysis, Data curation, Software, Validation, Writing – original draft. **Zhen Zhang:** Conceptualization, Methodology, Writing – original draft, Writing – review & editing, Funding acquisition, Project administration. **Bo Hao:** Data curation, Validation. **Shichuan Wei:** Investigation, Validation. **Yu Huang:** Resources, Supervision. **Guojun Zhang:** Supervision, Funding acquisition, Project administration.

Declaration of competing interest

The authors declare that they have no known competing financial interests or personal relationships that could have appeared to influence the work reported in this paper.

Data availability

Data will be made available on request.

Acknowledgments

This research is funded by Key Laboratory of Icing and Anti/De-icing of CARDC, China (Grant No. IADL20220411), National Natural Science Foundation of China under Grant No. 51975228, Innovative and Research Team Project of Guangdong Pearl River Talents Program, China under Grant No. 2017BT01G167. In addition, this research is also supported by Guangdong Basic and Applied Basic Research Foundation, China under Grant No. 2022A1515140083

References

- [1] Altin Karataş M, Gökkaya H. A review on machinability of carbon fiber reinforced polymer (CFRP) and glass fiber reinforced polymer (GFRP) composite materials. *Def Technol* 2018;14:318–26.
- [2] Shahar FS, Hameed Sultan MT, Lee SH, Jawaaid M, Md Shah AU, Safri SNA, et al. A review on the orthotics and prosthetics and the potential of kenaf composites as alternative materials for ankle-foot orthosis. *J Mech Behav Biomed Mater* 2019;99:169–85.
- [3] Scholz MS, Blanchfield JP, Bloom LD, Coburn BH, Elkington M, Fuller JD, et al. The use of composite materials in modern orthopaedic medicine and prosthetic devices: A review. *Compos Sci Technol* 2011;71:1791–803.
- [4] Joshi S, Rawat K, B ASS. A novel approach to predict the delamination factor for dry and cryogenic drilling of CFRP. *J Mater Process Technol* 2018;262:521–31.
- [5] Póor D, Geier N, Pereszlai C, Xu J. A critical review of the drilling of CFRP composites: Burr formation, characterisation and challenges. *Composites B* 2021;223:109155.
- [6] Geier N, Davim JP, Szalay T. Advanced cutting tools and technologies for drilling carbon fibre reinforced polymer (CFRP) composites: A review. *Composites A* 2019;125:105552.
- [7] Dang J, Zou F, Cai X, An Q, Ming W, Chen M. Experimental investigation on mechanical drilling of a newly developed CFRP/Al co-cured material. *Int J Adv Manuf Technol* 2020;106:993–1004.
- [8] Cao S, Li H, Tan G, Wu C, et al. Bi-directional drilling of CFRPs: From principle to delamination suppression. *Composites B* 2023;248:110385.
- [9] Kumar R, Agrawal PK, Singh I. Fabrication of micro holes in CFRP laminates using EDM. *J Manuf Process* 2018;31:859–66.
- [10] Roldan-Jimenez L, Bañon F, Valerga AP, Fernandez-Vidal SR. Design and analysis of CFRP drilling by electrical discharge machining. *Polymers* 2022;14:1340.

- [11] Shanmugam DK, Nguyen T, Wang J. A study of delamination on graphite/epoxy composites in abrasive waterjet machining. *Composites A* 2008;39:923–9.
- [12] Zhang Z, Liu D, Zhang Y, Xue T, Huang Y, Zhang G. Fabrication and droplet impact performance of superhydrophobic Ti6Al4V surface by laser induced plasma micro-machining. *Appl Surf Sci* 2022;605:154661.
- [13] Ming W, Sun P, Zhang Z, Qiu W, Du J, Li X, et al. A systematic review of machine learning methods applied to fuel cells in performance evaluation, durability prediction, and application monitoring. *Int J Hydrogen Energy* 2023;48:5197–228.
- [14] Akman E, Bora MÖ, Çoban O, Oztoprak BG. Laser-induced groove optimization for Al/CFRP adhesive joint strength. *Int J Adhes Adhes* 2021;107:102830.
- [15] El-Hofy MH, El-Hofy H. Laser beam machining of carbon fiber reinforced composites: a review. *Int J Adv Manuf Technol* 2019;101:2965–75.
- [16] Zhang Z, Qiu W, Zhang G, Liu D, Wang P, et al. Progress in applications of shockwave induced by short pulsed laser on surface processing. *Opt Laser Technol* 2023;157:108760.
- [17] Hejjaji A, Singh D, Kubher S, Kalyanasundaram D, Gururaja S. Machining damage in FRPs: Laser versus conventional drilling. *Composites A* 2016;82:42–52.
- [18] Wang P, Zhang Z, Liu D, Qiu W, Zhang Y, Zhang G. Comparative investigations on machinability and surface integrity of CFRP plate by picosecond laser vs laser induced plasma micro-drilling. *Opt Laser Technol* 2022;151:108022.
- [19] Tao N, Chen G, Fan L, Wang B, Li M, Fang W. Temperature-dependent material removal during pulsed laser processing of CFRP composites. *Opt Laser Technol* 2021;144:107445.
- [20] Xu H, Hu J. Study of polymer matrix degradation behavior in CFRP short pulsed laser processing. *Polymers* 2016;8:299.
- [21] Leone C, Mingione E, Genna S. Laser cutting of CFRP by quasi-continuous wave (QCW) fibre laser: Effect of process parameters and analysis of the HAZ index. *Composites B* 2021;224:109146.
- [22] Ohkubo T, Sato Y, Matsunaga E, Tsukamoto M. Three-dimensional numerical simulation during laser processing of CFRP. *Appl Surf Sci* 2017;417:104–7.
- [23] Yang H, Liu H, Gao R, Liu X, Yu X, Song F, et al. Numerical simulation of paint stripping on CFRP by pulsed laser. *Opt Laser Technol* 2022;145:107450.
- [24] Contuzzi N, Casalino G. Statistical modelling and optimization of nanosecond Nd: YAG Q-switched laser scarfing of carbon fiber reinforced polymer. *Opt Laser Technol* 2022;147:107599.
- [25] Li W, Huang Y, Chen L, Chen X, Zhang G, Rong Y. Effect of anisotropy on the quality of laser cutting corner of CFRP plate. *ASME J Manuf Sci Eng* 2022;144(11):111003.
- [26] Ohkubo T, Tsukamoto M, Sato Y. Numerical simulation of laser beam cutting of carbon fiber reinforced plastics. *Physics Procedia* 2014;56:1165–70.
- [27] Takahashi T, Tsukamoto M, Masuno S, Sato Y. Heat conduction analysis of laser CFRP processing with IR and UV laser light. *Composites A* 2016;84:114–22.
- [28] Romoli L, Fischer F, Kling R. A study on UV laser drilling of PEEK reinforced with carbon fibers. *Opt Lasers Eng* 2012;50(3):449–57.
- [29] Zhou C, Li H, Chen G, Wang G, Shan Z. Effect of single pulsed picosecond and 100 nanosecond laser cleaning on surface morphology and welding quality of aluminium alloy. *Opt Laser Technol* 2020;127:106197.
- [30] Wang J, Yang Y, Qi J, Liu Z, Zhou L. Thermodynamic simulation, surface morphology and bending property of carbon fiber reinforced polymer composite material subjected to laser cleaning. *Opt Laser Technol* 2022;152:108099.
- [31] Jiao J, Wang X. A numerical simulation of machining glass by dual CO2-laser beams. *Opt Laser Technol* 2008;40:297–301.
- [32] Yin J, Cao Y, Cui Y, Lu L, Yan Y, Chen J. Nd: YAG laser ablation of aluminum alloy 6061 before and after silicon dioxide coating. *J Alloys Compd* 2021;877:160329.
- [33] Xu H, Hu J. Modeling of the material removal and heat affected zone formation in CFRP short pulsed laser processing. *Appl Math Model* 2017;46:354–64.
- [34] Zhang G, Hua X, Huang Y, Zhang Y, Li F, Shen C, et al. Investigation on mechanism of oxide removal and plasma behavior during laser cleaning on aluminum alloy. *Appl Surf Sci* 2020;506:144666.
- [35] Xu L, Lu J, Li K, Hu J. Removal mechanism of CFRP by laser multi direction interaction. *Opt Laser Technol* 2021;143:107281.
- [36] Li W, Zhang G, Huang Y, Rong Y. UV laser high-quality drilling of CFRP plate with a new interlaced scanning mode. *Compos Struct* 2021;273:114258.
- [37] Geier N, Patra K, Anand R, et al. A critical review on mechanical micro-drilling of glass and carbon fibre reinforced polymer (GFRP and CFRP) composites. *Composites B* 2023;254:110589.